Finite Elements in Analysis and Design 92 (2014) 72–79

Contents lists available at ScienceDirect

Finite Elements in Analysis and Design

journal homepage: www.elsevier.com/locate/finel

Experimental and numerical study of laser-assisted machining of Ti6Al4V titanium alloy

Y. Ayed [a,b,*], G. Germain [a], W. Ben Salem [c], H. Hamdi [b]

[a] Arts et Métiers ParisTech, LAMPA, 2 bd du Ronceray, 49035 Angers Cedex, France
[b] Ecole Nationale dIngénieurs de Saint-Etienne, LTDS 58 rue Jean Parot, 42023 Saint-Etienne, France
[c] Ecole Nationale dIngénieurs de Monastir, LGM, Tunisie

ARTICLE INFO

Article history:
Received 25 March 2013
Received in revised form
13 July 2014
Accepted 12 August 2014
Available online 7 September 2014

Keywords:
Laser assisted machining
Numerical simulation
Chip formation
Titanium machining
Adiabatic shear band

ABSTRACT

Laser-assisted machining combines several experimental parameters such as cutting speed, feed rate, depth of cut, laser power and distance between tool rake face and the laser beam axis. The optimization of these parameters is necessary to ensure the efficiency of assistance and to increase productivity. This paper focuses on the understanding of the physical phenomena during laser-assisted machining, and on optimising this process. This contribution is based on an experimental and a numerical study. The experimentalpart highlights the effects of the laser power as well as the distance between the tool rake face and the axis of the laser beam. As for the numerical part, it was performed on the ABAQUS/Explicit software.

The proposed model improves the understanding of the physical phenomena of chip formation and the cutting force reduction when machining with laser assistance. In addition, this model allows a better optimization of laser and cutting parameters.Numerical findings generally corroborate experimental results and can lead to some other information difficult to catch experimentally.

The main contention in the paper is that the distance between the axis of the laser beam and the tool rake face is the most important parameter that controls the reduction of the cutting force. This cutting force reduction can exceed 50%.

1. Introduction

Titanium alloys are known for their high mechanical characteristics even at high temperatures and for their corrosion resistance. Besides, some of them are biologically compatible with the human body. The combination of high mechanical properties, low density and corrosion resistance presents interesting advantages for titanium alloys. However, they are difficult to machine. This is mainly due to the significant release of heat in the cutting area and the high chemical reactivity of titanium alloys that not only cause a rapid wear of cutting tools, but also generate very high cutting forces.

Therefore, research has been oriented to machining assistance in order to improve the machinability of these alloys and increase productivity. Skvarenina and Shin [1] studied the laser assisted-machining of graphite iron. The study shown an increase in tool life up to 60% and a saving in economic cost around 20%. The microstructure of the finished surface was not affected. Chang and Kuo [2] found that laser assistance contributes to the improvement of surface roughness and leads to a higher material removal rate when machining an aluminum oxide ceramic.

The study done by Ding and Shin [3] proves that there is an improvement in surface roughness and that there is no microstructural change. In addition there is more compressive surface axial residual stress and about 20% of reduction in the cutting force [4]. The numerical simulation of laser-assisted micro-milling process done by [4] shows that the flow stress drops by 20–25% and that there is a reduction in tool wear.

Numerical simulation of assisted machining processes is even more complex because it involves the coupling of multi-physic phenomena. Lesourd [5] was among the first to develop a finite element model for laser-assisted machining (LAM). This model takes into account laser heating by a uniform initial temperature imposed on the workpiece depending on the laser power used. His model predicted the morphology of the chip, the shear angle and temperature fields for the titanium alloy Ti6Al4V. A new model taking into account the temperature field induced by the laser beam has been developed by Germain [6]. This model allows the heating of the workpiece by a moving heat source, then the removal of material by a cutting tool. This new model allows the prediction of the stress levels, strain rates and temperature fields

* Corresponding author.
E-mail address: ayed.yessine@hotmail.fr (Y. Ayed).

http://dx.doi.org/10.1016/j.finel.2014.08.006
0168-874X/

in the cutting zone in conventional machining (CM) and in LAM. Based on the research carried out by Mabrouki [7,8], the model proposed by Germain can begreatly improved. Thus, the understanding of laser heating on the chip formation becomes more relevant. The main objective of this study is to determine the effects of cutting parameters and those of the laser source on the chip formation and the cutting force.

2. Orthogonal cutting simulation and shear band formation

2.1. Geometric model

The geometric model proposed consists of a carbide cutting tool and a part made of Titanium alloy Ti6Al4V.

The adopted geometric model for the workpiece (length = 5 mm), presented in Fig. 1, follows the main geometric multi-part model suggested in [7]. It has different parts: part one (1) it is transformed into a chip during machining, part two (2) represents the material separation zone, part three (3) is the area of the part remaining after machining. The tungsten carbide tool is considered deformable, flank angle $\alpha = 7^\circ$, rake angle $\gamma = -7^\circ$ and nose radius $r_\beta = 30\ \mu m$.

A master-slave contact algorithm is used. Frictional behavior of the interface is modelled according to the identification done by [9]. This model is meshed by 4-node quadrangle elements (CPE4RT) of about 12 μm in the cutting area (according to [9]). The total number of elements is about 9200. The calculation type is Explicit Coupled-Temperature-Displacement under the assumption of plane strain condition (2D).

2.2. Material constitutive and damage laws

The workpiece behavior law must take into account all physical aspects that may occur during machining (high strain rates and high temperatures). The tool is modelled by an elastic law. The physical parameters of the workpiece and the tool are given by Table 1.

In a cutting operation, strain rates are important, their estimation by analytical and experimental methods is of the order of $10^3\ s^1$–$10^5\ s^1$ [18,19]. When the strain rate increases, the flow stress also increases leading to the generation of heat due to plastic deformation. It is, therefore, crucial to choose a constitutive equation which takes into account the influence of strain hardening, strain rate and temperature. One of the most widely used behavior laws is the Johnson–Cook constitutive equation (1) [10].

$$\sigma = \underbrace{(A + B\dot{\bar{\varepsilon}}^n)}_{1} \underbrace{\left(1 + C \ln\left(\frac{\dot{\bar{\varepsilon}}}{\dot{\bar{\varepsilon}}_0}\right)\right)}_{2} \underbrace{\left(1 - \left(\frac{T - T_{room}}{T_{fusion} - T_{room}}\right)^m\right)}_{3} \quad (1)$$

The first term in Eq. (1) corresponds to the hardening, A is the yield stress, B and n are the hardening parameters. The second term represents the effect of the strain rate as a function of the parameter C. The third term refers to the thermal softening where m is the temperature sensitivity. The determination of these five parameters requires quasi-static and dynamic tests at different strain rates and temperatures. In the current study, these parameters are taken from bibliography [12].

Johnson and Cook [11] have developed in the mid 1980s a damage model which takes into account the sensitivity to strain rate, temperature and hydrostatic pressure . That law is described

Table 1
Physical parameters of the workpiece and the cutting tool [9].

Physical parameters	Workpiece (Ti6Al4V)	Tool (tungsten carbide)
Elastic modulus E(GPa)	110	705
Poisson's ratio ν	0.33	0.23
Density ρ(kg/m^3)	4430	15,700
Thermal conductivity λ(W/m °C)	6.6	24
Specific heat C_p(J/kg °C)	670	178

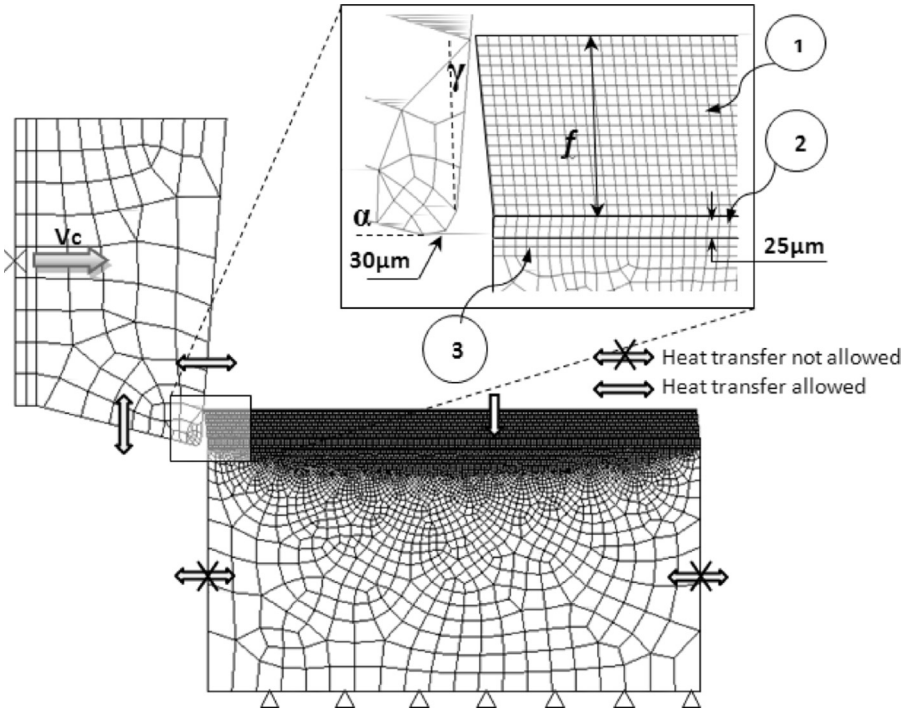

Fig. 1. Geometric model.

in Eqs. (2) and (3).

$$D = \sum \frac{\Delta\varepsilon}{\varepsilon^f} \tag{2}$$

$$\varepsilon^f = \underbrace{(D_1 + D_2 \exp(D_3\sigma^*))}_{1} \underbrace{\left(1 + D_4 \ln\left(\frac{\dot{\bar{\varepsilon}}}{\dot{\bar{\varepsilon}}_0}\right)\right)}_{2} \underbrace{\left(1 + D_5\left(\frac{T - T_{room}}{T_{fusion} - T_{room}}\right)\right)}_{3} \tag{3}$$

$\Delta\varepsilon$ is the increment of the equivalent plastic strain, ε^f is the equivalent strain at fracture. The variable D is calculated at each increment for each mesh element, the initiation of damage occurs when $D=1$.

The first term in Eq. (3) is based on the calculation of the rate of tri-axiality. Indeed, when the hydrostatic pressure increases, the fracture strain decreases. The second term and the third term represent, respectively, the sensitivity to the strain rate and temperature. The damage is based on the stiffness degradation of the material until failure point. Table 2 illustrates the parameters of the behavior and the damage law used.

Table 2
Johnson–Cook behavior and damage law parameters [12,13].

A (MPa)	B (MPa)	n	C	m	$\dot{\varepsilon}_0(s^{-1})$	D_1	D_2	D_3	D_4	D_5
782.7	498.4	0.28	0.028	1.0	10^{-5}	−0.09	0.25	−0.5	0.014	3.87

2.3. Shear band formation

The model allows, among others, to simulate the formation of shear bands during chip genesis. Fig. 2 shows the steps of the formation of a shear band. The variation of the temperature and the von Mises stress during the formation of a shear band are plotted at point P. Point P is positioned in the middle of the shear band (it is attached to the Lagrangian mesh (Fig. 2).

Poulachon et al. [14] studied the formation of shear bands for a AISI 52100 steel basing on an instability criterion. He concluded that the instability of shear is more sensitive to an increase in flow stress than changes in thermal properties. Delalondre [15] explains the occurrence of adiabatic shear bands (ASB) by three phases:

1. A period of plastic deformation: During this phase the distribution of plastic deformation is homogeneous and the phenomenon of hardening outweighs the softening phenomenon. At the end of this phase the maximum stress is reached.
2. A period of initiation of the ASB: The hardening and softening phenomena have comparable intensities.
3. A period of establishment of the ASB: The equivalent stress drops abruptly under the influence of the thermal softening that dominates it. At this stage, the temperature rises sharply in the ASB. For the ASB that is formed, the temperature reaches its maximum and the stress reaches its minimum.

These three phases correspond to the results found (Fig. 2). Indeed, phase 1 corresponds to Step 1. Phase 2 represents the transition from Step 1 to Step 2. Phase 3 corresponds to Step 2. Step 3 corresponds to the shear propagation throughout the shear band.

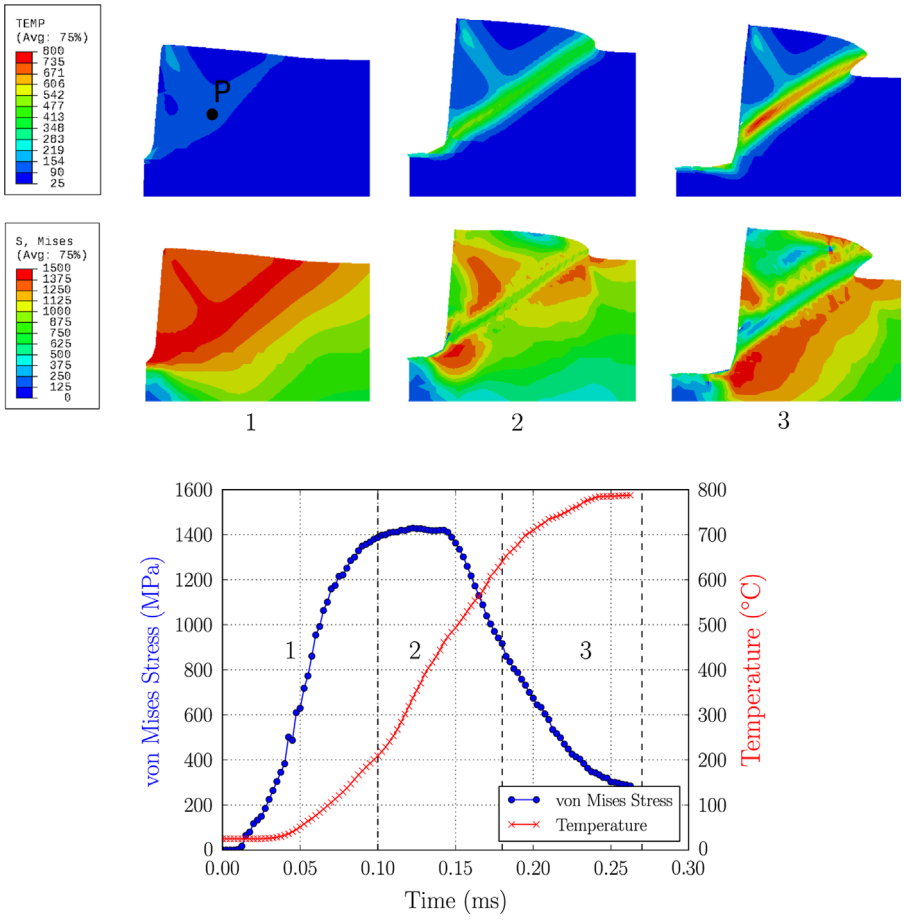

Fig. 2. Shear band formation.

3. Numerical simulation of laser heating

3.1. Modeling

Physically, laser heating is carried out by the absorption of the laser beam on only few nanometers. Laser heating modeling can be performed by applying a surface heat flux. In fact, the energy of the laser used is not completely absorbed by the material: a fraction is reflected and a complementary fraction is absorbed. The absorptivity depends on several factors: the nature of the machined material, the laser wavelength, its intensity, the workpiece roughness and surface oxidation [16]. The heat flux will be imposed equally to the heat absorbed by the part.

A moving heat flux using the DFLUX subroutine is applied to the same workpiece used in the cutting model in order to keep the same geometry and the same mesh. Eq. (4) presents the programmed heat flux.

$$Q(r) = \frac{3P}{\pi r_1^2} \exp\left(-3\frac{r^2}{r_1}\right) \tag{4}$$

- r_1: radius of the laser spot
- P: laser power
- Q: heat generated by the laser source
- $r = x^2 + y^2$ (x and y axes)

An initial temperature of 25 °C is imposed on the workpiece. Purely thermal simulations are done. The heat flux moves on the surface of the workpiece at a speed which corresponds to the cutting speed.

3.2. Numerical results

3.2.1. Thermal field induced by the laser heating

The laser produces an intense and a localized heat. The temperature field depends mainly on the speed, power, and diameter of the incident beam. Fig. 3 illustrates the temperature fields at different speeds and different laser powers for a laser beam of 0.8 mm in diameter (all temperatures are in °C).

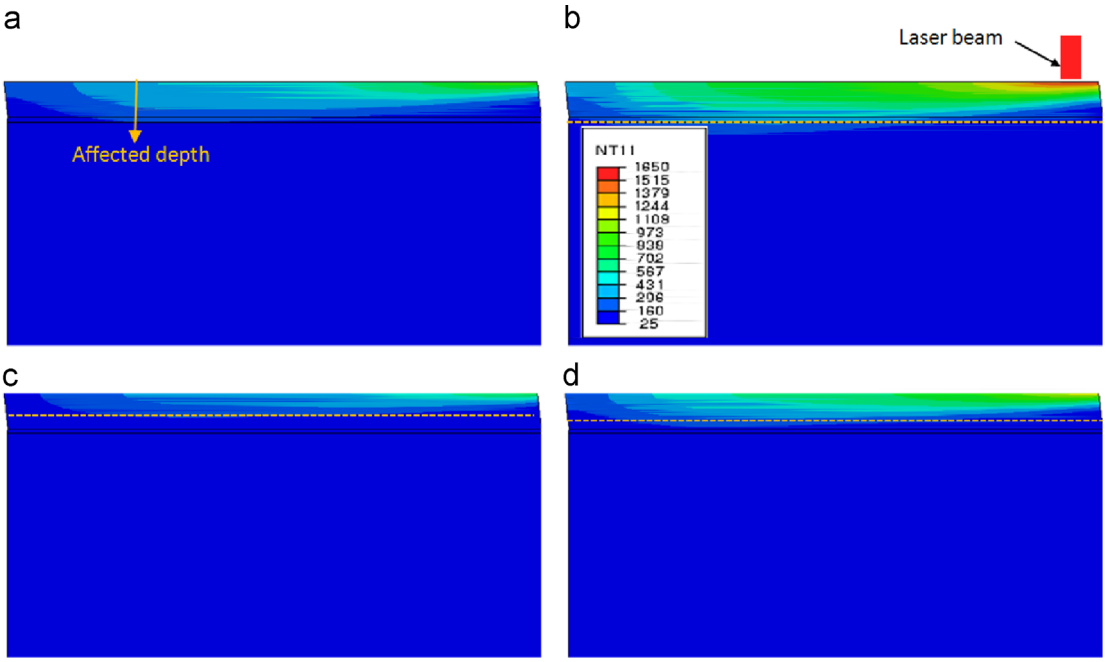

Fig. 3. Thermal field induced by laser heating, (a) $V=0.66$ m/s, $P=500$ W, (b) $V=0.66$ m/s, $P=1000$ W, (c) $V=1.33$ m/s, $P=500$ W, (d) $V=1.33$ m/s, $P=1000$ W.

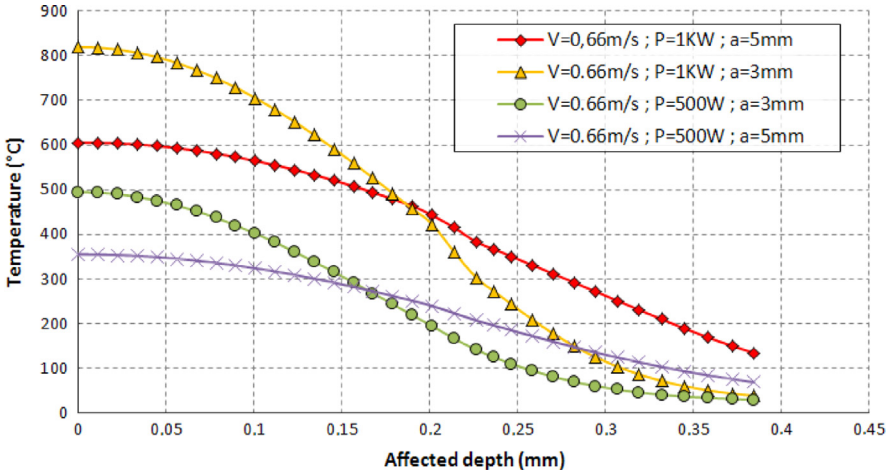

Fig. 4. Affected depth.

Temperature fields (a) and (c) have the same power level but with different speeds respectively 0.66 m/s and 1.3 m/s. The affected depth and the maximum temperature reached decrease when the speed increases. In fact, the increase in displacement speed decreases the laser-material interaction time. Temperature fields (a) and (b) correspond to the results for the same speed but with different laser powers. In this case, it is found that the maximum temperature increases with the laser power. The interaction time is identical for both simulations but power density is larger which allows to reach higher temperatures with a higher energy intensity. By contrast, the heat-affected depth is almost identical.

3.2.2. Optimization of laser/tool distance

The efficiency of the laser heating depends essentially on the distance between the axis of the laser beam and the tool rake face. In fact, the purely thermal simulation described previously, allows us to know the optimal distance between the tool and the laser beam. The distance is considered to be optimal when the reduction of the cutting force is maximized and the affected depth by the laser beam is removed by the cutting tool.

The depth affected by the heating depends mainly on the speed of the laser beam, its power and the distance a between the cutting face of the tool and the beam axis. For this, heating simulations were made by varying the distance a and the power of the laser source. For example, for a speed of 0.66 m/s, Fig. 4 illustrates the variation in temperature as a function of the affected depth.

This demonstrates that a larger gain in cutting force is expected for all cutting depths below 0.15 mm if a distance of 3 mm and a laser power of 1000 W are chosen. However, for the cutting depths up to 0.2 mm a slight reduction is expected when using a laser power of 500 W. This reduction will not be significant because the temperature levels are not enough to soften the material. Thus, for higher cutting depths, the laser power must be upgraded.

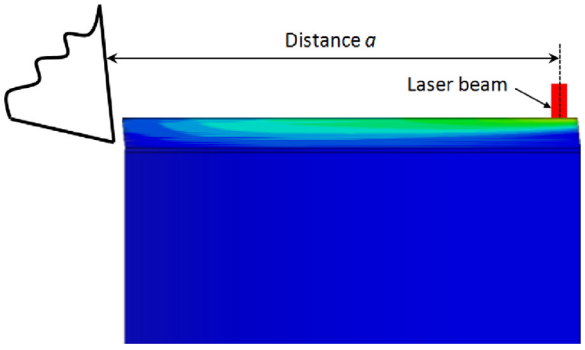

Fig. 5. A schematic presentation of the LAM model.

4. Numerical simulation of laser-assisted machining

4.1. Modeling approach

The modelisation of LAM is the result of coupling the two previous models. Thus, it requires a simulation of the laser heating then the introduction of the thermal field obtained as an initial condition for the orthogonal cutting model. The contact between the tool and the workpiece is handled by a master–slave algorithm. A frictional heating has been taken into account [9]. Fig. 5 illustrates the LAM model.

4.2. Results

The main objective of the simulation of the LAM is to study the influence of heating on the chip formation. Fig. 6 shows an example of simulation, at the same time, under the same cutting conditions in CM (Fig. 6 (a)) and in LAM (Fig. 6 (b)).

Particular attention was paid to the temperature evolution in the tool and the workpiece. Fig. 7 shows the temperature fields in different conditions at a point of the tool rake face. In LAM, for a cutting speed of about 80 m/min the average temperature of the material that will be machined, just before the primary zone, is approximately 350 °C at 500 W and 600 °C at 1000 W. In these conditions, temperature of the tool is not strongly influenced by the laser power (Fig. 7d). It is, therefore, possible to have an effect of the laser assistance on the chip formation without an excessive thermal loading of the tool.

However, Fig. 8 demonstrates that the heat flux (W/mm^2) induced by plastic deformation in LAM conditions is less than the heat flux generated in CM condition. This reduction is due to the decrease of the flow stress caused by laser heating.

5. Experimental study

5.1. Macroscopic point of view

The machine used is a dedicated hard turning REALMECA RT-5, modified to receive the focusing laser head on a specific gantry (5 axes). The laser source used is Nd: YAG laser with a maximum power of 2.5 kW. The acquisition of the components of the cutting forces is obtained using a Kistler dynamometer (9257B): F_t is the cutting force (tangential force) and F_r is the radial force. The diagram of the experimental setup is shown in Fig. 9.

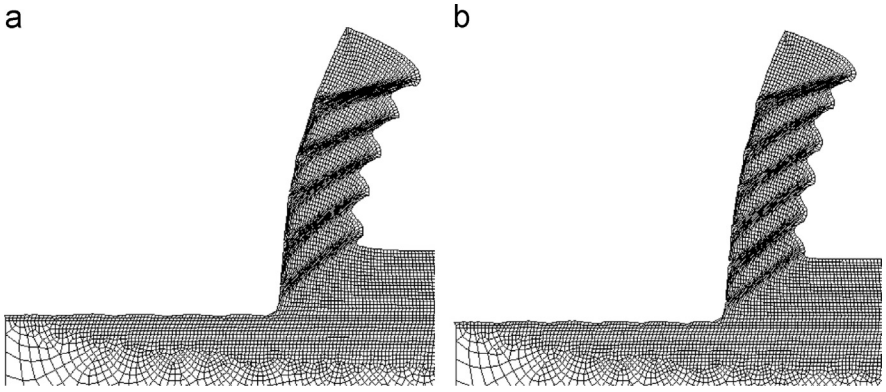

Fig. 6. Chip morphology for two different configurations, (a) Vc=80 m/min, f=0.2 mm/rev, (b) Vc=80 m/min, f=0.2 mm/rev, P=500 W.

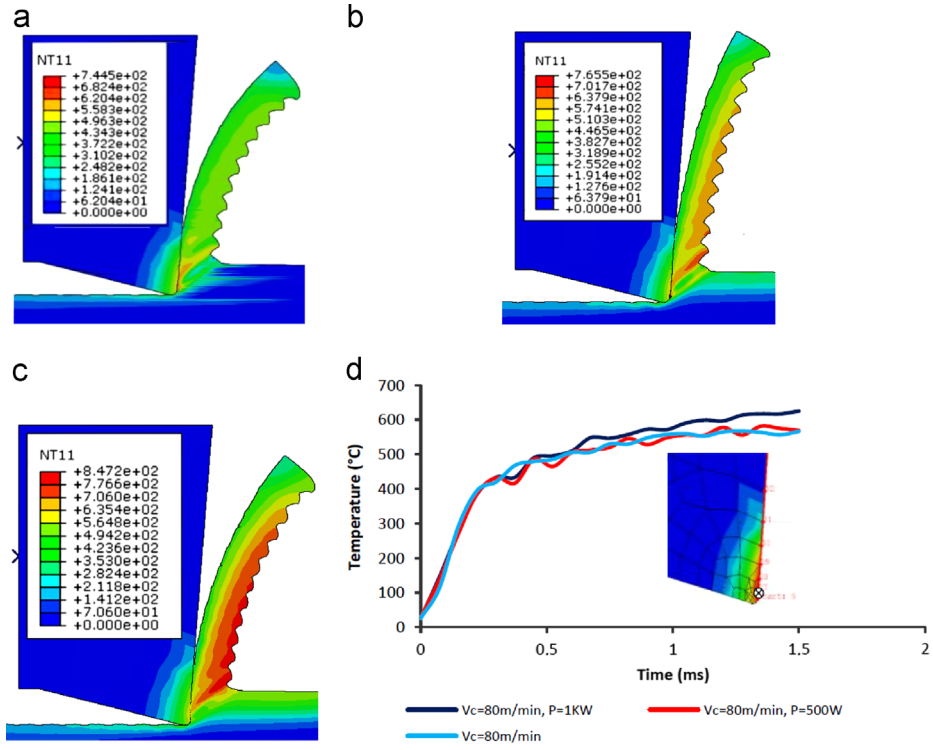

Fig. 7. Thermal fields for three configurations, (a) Vc=80 m/min, f=0.2 mm/rev, (b) Vc=80 m/min, f=0.2 mm/rev, P=500 W, (c) Vc=80 m/min, f=0.2 mm/rev, P=1000 W, (d) Temperature evolution in the tool cutting face.

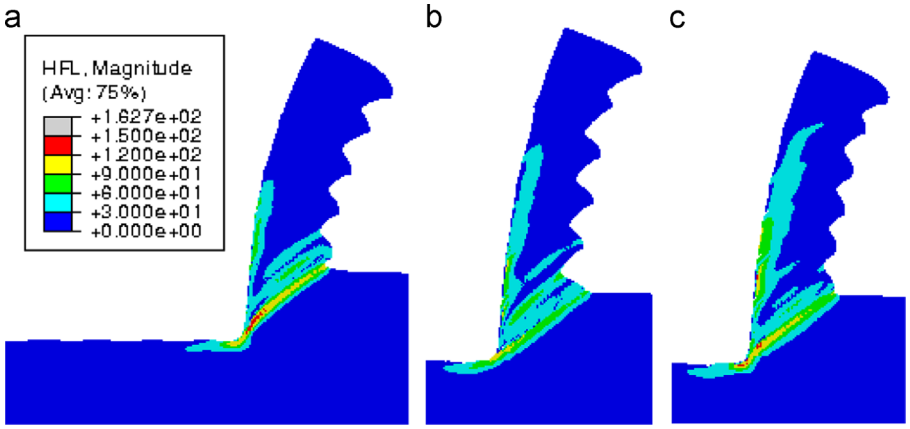

Fig. 8. Heat flux induced by plasticdissipation for three conditions. (a) Vc=80 m/min, f=0.2 mm/rev, (b) Vc=80 m/min, f=0.2 mm/rev, P=500 W (c) Vc=80 m/min, f=0.2 mm/rev, P=1000 W.

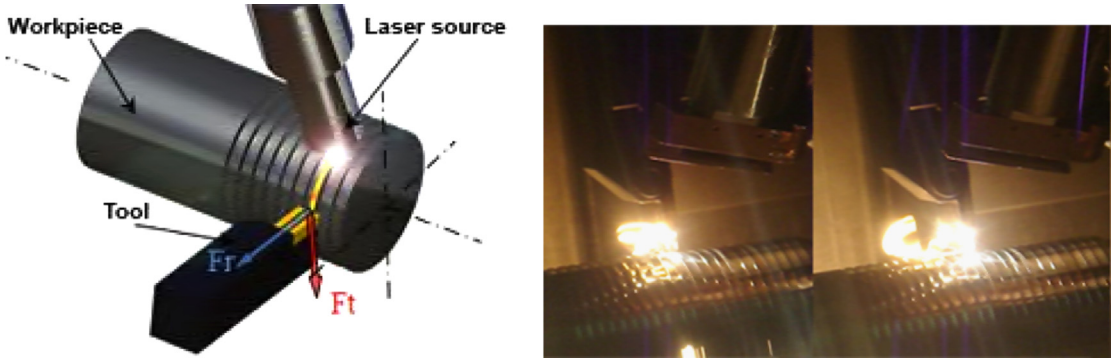

Fig. 9. Experimental setup.

Tests were conducted on the basis of an experimental design plan that covers a wide range of cutting conditions and parameters of the laser source. Table 3 summarizes the main results retained.

These experimental results show a reduction of the cutting forces (F_t), varying from 4% to 55%. This reduction depends on the cutting parameters and the laser source. This can be explained by the laser material interaction time required to degrade the mechanical properties of the material and the laser power. This is the effect of the thermal softening of the material. Moreover, this effort reduction is even greater when the laser power is increased. However, an increase in the cutting speed or in the feed rate leads to a decrease in the rate of reduction in the cutting forces. The power control of the laser beam and the distance between the laser beam axis and the tool cutting face is decisive. In most circumstances, the adjustment of the distance to about 5 mm is more effective in reducing the cutting force. Let us consider the two following cases:

- Vc=40 m/min, f=0.1 mm/rev and P=500 W: The reduction of the cutting force is more important when the distance a is fixed to 5 mm than a distance of 3 mm, the reduction rate is respectively 37% and 25%.
- Vc=40 m/min, f=0.2 mm/rev, P=1000 W : There is a significant reduction of the cutting force which exceed 50%. When a=3 mm and P=1000 W there is a local melting of the chip. It sticks on the rake face of the tool changing the contact between the tool and the chip.

Table 3
Main experimental results (cutting depth 1 mm).

	P(W)	a(mm)	f(mm/rev)	Vc(m/min)	F_t(N)
Conventional			0.2	40	380
Assisted	500	5	0.2	40	320
	500	3	0.2	40	321
	1000	5	0.2	40	213
	1000	3	0.2	40	278
Conventional			0.1	40	270
Assisted	500	5	0.1	40	170
	500	3	0.1	40	200
	1000	5	0.1	40	130
	1000	3	0.1	40	117
Conventional			0.1	80	262
Assisted	500	5	0.1	80	191
	500	3	0.1	80	182
	1000	5	0.1	80	151
	1000	3	0.1	80	144
Conventional			0.2	80	343
Assisted	500	5	0.2	80	317
	500	3	0.2	80	338
	1000	5	0.2	80	284
	1000	3	0.2	80	294

Fig. 10(a) shows that for a feed rate of 0.1 mm/rev, the reduction of the cutting force is important regardless of the machining conditions and the laser parameters. Increasing the cutting speed affects this rate of reduction without affecting significantly the efficiency of the laser assistance. Moreover, Fig. 10(b) shows that for a feed rate of 0.2 mm/rev, assistance efficiency drops, particularly at the power of 500 W. Doubling the cutting speed, laser assistance becomes almost ineffective. However, the increase of the laser power can improve the rate of reduction of the cutting force. A maximum reduction is obtained when a is fixed to 5 mm.

Increasing the laser power leads to a better rate of reduction of the cutting force. However, this could cause the melting and the bonding of the chip on the rake face of the tool. This increase appears to be more effective when the cutting speed or feed rate is increased.

5.2. Microscopic point of view

The chips were carefully analyzed.The micrographic analysis of samples is based on the comparison of the obtained chip morphology. This shows remarkable differences between the chips obtained by conventional machining tests and those obtained by laser-assisted machining tests. Fig. 11 shows micrographs obtained from different cutting conditions and different laser parameters.

Microscopic observations show a sawtooth shape of the chip for all the tested conditions. Fig. 11 shows the presence of shear bands, the magnification of imagesevidences the deformation of the grains. Table 4 shows a comparison between the geometrical parameters of the chip for various cutting conditions and different powers of the laser beam. Thus, the shear angle decreases when increasing the temperature, which causes an increase in the average chip thickness. This confirms the results of Lesourd [5] and Germain [17].

From Table 4, it can be concluded that, regardless to the cutting conditions used, the increase in the laser power leads to the decrease of the shear angle and the increase of the chip thickness. Moreover, the distance Dc (Fig. 11) tends to decrease when heat is increased. These changes in the shear angle ϕ and the distance Dc

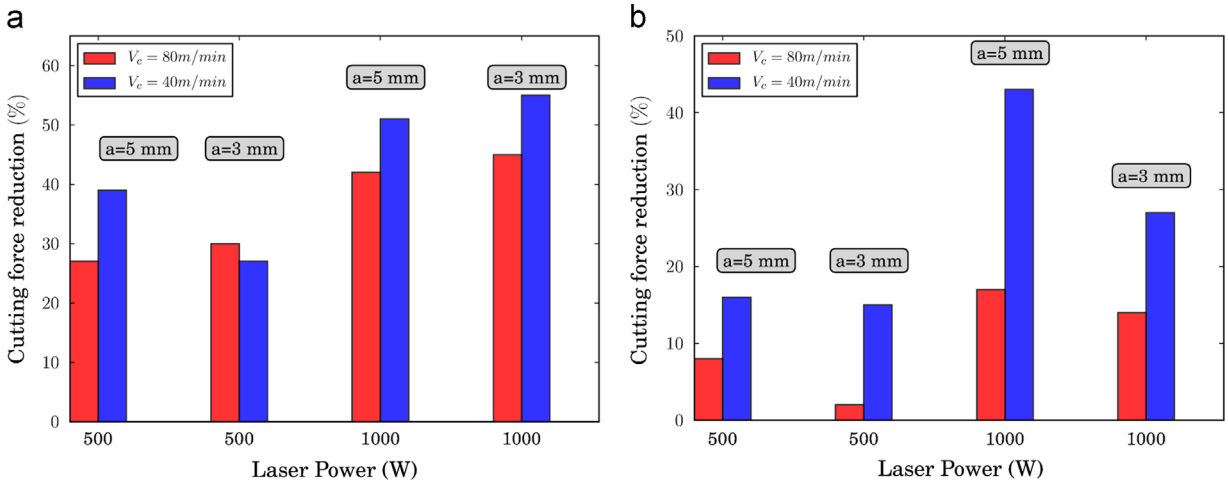

Fig. 10. Cutting force reduction, (a) f=0.1 mm/rev , (b) f=0.2 mm/rev.

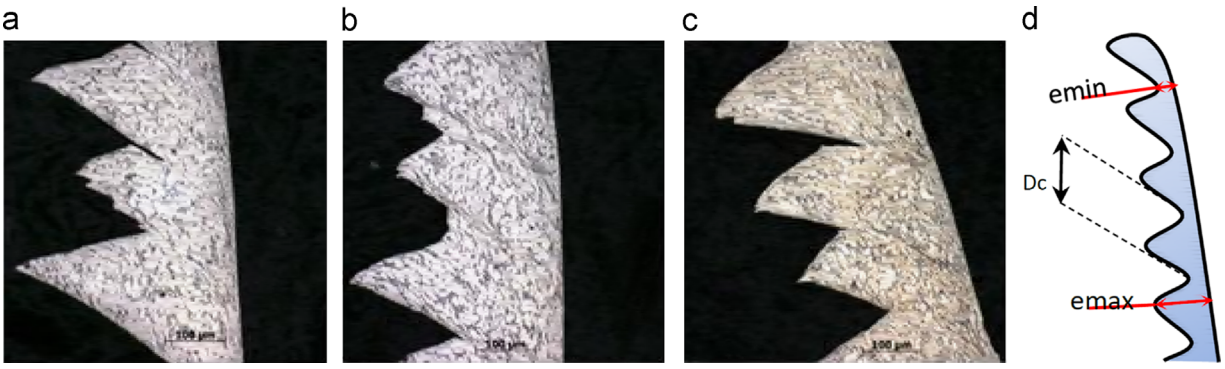

Fig. 11. Chip morphology for different laser powers: Vc=40 m/min, f=0.2 mm/rev (a) CM (b) LAM P=500 W (c) LAM P=1000 W, (d) chip morphology illustration.

Table 4
Geometrical parameters of the chip and cutting force (Vc=80 m/min, f=0.2 mm/rev).

P (W)	e_{min} (μm)	e_{max} (μm)	D_C (μm)	ϕ (Exp)	ϕ (Num)	Fc (Exp)	Fc (Num)
CM	124	287	233	39	42	343	380
LAM 500	180	348	140	37	34	338	329
LAM1000	160	370	105	31	28	294	306

generate an increased frequency of segmentation of the chip. Numerical results confirm the microscopic observations.

In conventional machining, during the formation of the shear band, the von Mises stress increases until it reaches a certain limit, a part of the plastic deformation energy is dissipated in the shear band causing thermal softening.

In laser-assisted machining the phenomenon of strain localization is always present with a higher frequency of the appearance of shear bands. This can be explained by the fact that the material has a higher temperature initially and reaches the yield stress of the material quickly.

6. Conclusion

A new cutting model was developed to understand the mechanics of chip formation in the case of laser-assisted machining.On the basis of a heating model, it was possible to optimize the laser parameters, in particular, the laser power and the distance between the laser beam axis and the tool rake face. The LAM model and the experimental study had highlighted the change in the geometry of the chip. The shear angle and the chip thickness decrease with the increase of the laser power. In addition, a significant reduction in the cutting force is also remarked. The amplitude of this reduction depends mainly on the cutting conditions and the laser characteristics. Higher cutting parameters require an increase of the power of the laser source. Changing cutting conditions and keeping the efficiency of assistance allows a significant increase of productivity.

References

[1] S. Skvarenina, Y. Shin, Laser-assisted machining of compacted graphite iron, Int. J. Mach. Tools Manuf. 46 (1) (2006) 7–17. http://dx.doi.org/10.1016/j.ijmachtools.2005.04.013.
[2] C.-W. Chang, C.-P. Kuo, Evaluation of surface roughness in laser-assisted machining of aluminum oxide ceramics with taguchi method, Int. J. Mach. Tools Manuf. 47 (1) (2007) 141–147. http://dx.doi.org/10.1016/j.ijmachtools.2006.02.009.
[3] H. Ding, Y.C. Shin, Laser-assisted machining of hardened steel parts with surface integrity analysis, Int. J. Mach. Tools Manuf. 50 (1) (2010) 106–114. http://dx.doi.org/10.1016/j.ijmachtools.2009.09.001.
[4] H. Ding, N. Shen, Y.C. Shin, Thermal and mechanical modeling analysis of laser-assisted micro-milling of difficult-to-machine alloys, J. Mater. Process. Technol. 212 (3) (2012) 601–613. http://dx.doi.org/10.1016/j.jmatprotec.2011.07.016.
[5] B. Lesourd, Etude et modélisation des mécanismes de bandes de cisaillement en coupe des métaux. application au tournage assisté laser de l'alliage de titane ta6v (Ph.D. thesis), Ecole Centrale de NANTES, 1996.
[6] G. Germain, P.D. Santo, J. Lebrun, Comprehension of chip formation in laser assisted machining, Int. J. Mach. Tools Manuf. 51 (3) (2011) 230–238. http://dx.doi.org/10.1016/j.ijmachtools.2010.11.006.
[7] T. Mabrouki, F. Girardin, M. Asad, J.-F. Rigal, Numerical and experimental study of dry cutting for an aeronautic aluminium alloy (a2024-t351), Int. J. Mach. Tools Manuf. 48 (11) (2008) 1187–1197. http://dx.doi.org/10.1016/j.ijmachtools.2008.03.013.
[8] T. Mabrouki, J.-F. Rigal, A contribution to a qualitative understanding of thermo-mechanical effects during chip formation in hard turning, J. Mater. Process. Technol. 176 (1–3) (2006) 214–221. http://dx.doi.org/10.1016/j.jmatprotec.2006.03.159.
[9] Y. Zhang, T. Mabrouki, D. Nelias, Y. Gong, Chip formation in orthogonal cutting considering interface limiting shear stress and damage evolution based on fracture energy approach, Finite Elem. Anal. Des. 47 (7) (2011) 850–863 http://dx.doi.org/10.1016/j.finel.2011.02.016.
[10] G. Johnson, W. Cook, A constitutive model and data for metals subjected to large strains, high strain rates and temperature, in: Seventh International Symposium on ballistics, 1983.
[11] G.R. Johnson, W.H. Cook, Fracture characteristics of three metals subjected to various strains, temperatures and pressures, Eng. Fract. Mech. 21 (1) (1985) 31–48. http://dx.doi.org/10.1016/0013-7944(85)90052-9.
[12] W.-S. Lee, C.-F. Lin, High-temperature deformation behaviour of ti6al4v alloy evaluated by high strain-rate compression tests, J. Mater. Process. Technol. 75 (1–3) (1998) 127–136. http://dx.doi.org/10.1016/S0924-0136(97)00302-6.
[13] D. Lesuer, Experimental investigations of material models for Ti-6Al-4 V Titanium and 2024-T3 Aluminum. Final Report, DOT/FAA/AR-00/25, US Department of Transportation, Federal Aviation Administration; 2000.
[14] G. Poulachon, A. Moisan, I. Jawahir, On modelling the influence of thermo-mechanical behavior in chip formation during hard turning of 100cr6 bearing steel, CIRP Ann. – Manuf. Technol. 50 (1) (2001) 31–36. http://dx.doi.org/10.1016/S0007-8506(07)62064-2.
[15] F. Delalondre, Modélisation et étude 3d des phénomènes de cisaillement adiabatiques dans les procédés de mise en forme grande vitesse (Ph.D. thesis), Ecole Nationale Supérieure des Mines de Paris, 2008.
[16] V. Steen, Laser Material Processing, Springer, New York, 1991.
[17] G. Germain, Contribution à l'optimisation du procédé d'usinage assistance laser (Ph.D. thesis), Arts et Metiers Paristech, 2006.
[18] G. List, G. Sutter, X. Bi, A. Molinari, A. Bouthiche, Strain, strain rate and velocity fields determination at very high cutting speed, J. Mater. Process. Technol. 213 (5) (2013) 693–699.
[19] J. Pujana, P. Arrazola, J. Villar, In-process high-speed photography applied to orthogonal turning, J. Mater. Process. Technol. 202 (1–3) (2008) 475–485.